HMM based Archive Film Defect Detection with Spatial and Temporal Constraints

Xiaosong Wang
http://www.cs.bris.ac.uk/~wang
Majid Mirmehdi
http://www.cs.bris.ac.uk/~majid

Department of Computer Science
University of Bristol
Bristol BS8 1UB, UK

Abstract

We propose a novel probabilistic approach to detect defects in digitized archive film, by combining temporal and spatial information across a number of frames. An HMM is trained for normal observation sequences and then applied within a framework to detect defective pixels by examining each new observation sequence and its subformations via a leave-one-out process. A two-stage false alarm elimination process is then applied on the resulting defect maps, comprising MRF modelling and localised feature tracking, which impose spatial and temporal constraints respectively. The proposed method is compared against state-of-the-art and industry-standard methods to demonstrate its superior detection rate.

1 Introduction

Restoration of old, archived films is of great importance to preserve the originality of the medium in terms of "a historical record" as well as the means to quality improvement for reproduction purposes. Helped by the development of mass-capacity digital storage technologies, most filmed footage, whether recently shot or historical, requires quality control and assessment in digital form before it gets broadcast or stored in a digital warehouse. This has resulted in growing industry interest in developing automated quality control for films and videos with several recent academic and industry collaborations in projects such as BRAVA (Broadcast Restoration of Archives by Video Analysis, 1999) [3] and PrestoSpace (Preservation towards Storage and access Standardised Practices for Audiovisual Contents in Europe, 2004) [14].

A variety of defects may occur in archived films. These were categorised in Project BRAVA [3] and include dirt, line scratches, brightness variation, and frame vibration amongst many others. The most common defect types are dirt and scratches which usually appear as black and white sparkles or regions in one or more frames. However, no common size or shape features can be deduced from these as their appearance is mostly random, caused by physical damage from inappropriate storage and handling [16]. Here, we shall refer to all such discontinuities, which appear across one or more frames, as dirt and sparkle, including salt and pepper like noise, blotches, and scratches.

In this paper, unlike previous methods, we examine longer temporal information at each pixel location and its neighbouring space. We assume the appearance of a defective pixel as

a stochastic pixel-change event and use HMM and MRF to model the temporal and spatial information respectively to obtain better results with fewer false detections. First, an HMM based Archive FIlm Defect detection method (HAFID) is presented. We train an HMM on normal observation sequences and then apply it within a framework to detect defective pixels by examining each new observation sequence and its subformations via a leave-one-out process. The resulting defect map from HAFID encapsulates the defects very well, but suffers from many false alarms. We therefore extend HAFID to add a two-stage false alarm elimination process and refer to the entire method as HAFID-STC (Spatial and Temporal Continuity analysis). First, the defect map from HAFID is modeled with a MRF to enforce spatial continuity constraints and then the pyramidal Lucas-Kanade feature tracker [2] is applied to impose temporal correlation constraints. We shall outline a comparison of HAFID-STC (and HAFID) against four commonly used and/or state-of-the-art techniques [8, 10, 12, 18][1]. The post defect detection stage of film restoration will be dealt with in our future work.

2 Background

Archive film defect detection methods can be broadly categorised into filter-based and model-based methods. Probably the earliest work on filter-based archive film defect detection is the BBC's hardware-based dirt and sparkle detector [21]. A binary defect map was generated by examining if the temporal forward and backward intensity differences are above a certain threshold. The Spike Detection Index (SDIp) [10] is another example of a filter like defect detector, which improved Storey's algorithm [21] by using motion compensated pixel values while requiring the forward and backward intensity differences to have the same sign. Nadenau and Mitra [13] also extended the work in [21] to use six pixel values from motion compensated temporal neighbours as $\{v_i | 1 \leq i \leq 6\}$. The algorithm sorted the six values as $\{s_i | 1 \leq i \leq 6\}$ and calculated the following three differences:

$$d_1 = |s_1 - s_6|; \quad d_2 = |s_2 - s_5|; \quad d_3 = |s_3 - s_4| \tag{1}$$

A defect was then marked if $d_1 > \tau_1$, $d_2 > \tau_2$ and $d_3 > \tau_3$ where $(\tau_i | i = 1,2,3)$ were thresholds. Other recent work includes Ren and Vlachos [17, 18] who created a confidence function of intensity differences to measure the possibility of a pixel being degraded. Image segmentation and local correlation information was also included to help eliminate false alarms. In [6, 7], Marshall and his co-workers dealt with small defects (within 7×7 windows) through direct restoration by using hierarchical soft morphological filters.

Model-based film defect detectors include works based on MRFs [5] where the central idea is to predict the intensity value of the target pixel by examining the intensity values of pixels in the neighbouring frames, *e.g.* [4, 12]. In [9, 11] a series of spatial-temporal Autoregressive (AR) models for defect detection were proposed, combined with restoration. In another AR model based work [20], instead of combining intensity values from both previous and next frames, Roosmalen interpolated the current pixel by using intensities from one direction only (either forward or backward) whose values were close to the predictions of his AR model. Kokaram [8] also developed a Bayesian framework to model noise and scratches while performing motion correction. Three binary variables were used for each pixel to mark if the pixel is degraded, forward occluded or backward occluded. These variables, together with restored image values and motion vectors, were defined as unknowns. Given the pixel

[1] Note although [10] is from 1992, it is still one of the most regularly used methods in industry.

values of degraded frames and initial motion estimations, the method applied the ICM [1] algorithm to solve these unknowns via an iterative procedure.

Traditionally, previous archive film defect detection methods have assumed defects only appear in single frames. This assumption is then followed by the practice of investigating the information from one or two previous and successive frames to determine if the current frame is suffering from degradation, *e.g.* the SDIp [10] and MRF based [11] detectors. The approach here is to look at a number of frames before and after the current frame. This allows us to examine the statistical changes in pixel transitions for a longer range to help determine defects more accurately. This will clearly incur extra computational costs, but this is nonetheless affordable for offline detection of defects in archival film. Indeed, we will show in Section 5 that our proposed method is computationally extremely competitive.

3 HMM based defect detection

In previous archive film defect detection methods, a common dilemma has been how to increase correct detection rates while reducing the number of false alarms. Given the somewhat random nature of the occurrence of defects, rather than attempting to model defects, we build a model of how normal a sequence of pixels is. This is in effect a form of novelty detection since any pixel sequences deviating from this normal model can be marked as a possible defect. A pixel $\mathbf{x}$ would normally remain in one state and undergo a transition only when the intensity value at this location changes by a certain amount. For example, a constant state sequence may be linked to a temporal pixel sequence at a static background, whereas a single frame based defect would cause sudden state transitions at that pixel location. This temporal change of states (at a pixel location) can be considered as a Markov chain. Given some observation sequences, we are then able to model normal pixel sequences (i.e. state transitions) using an HMM.

To begin with, we train a single HMM, θ, for normal image pixel sequences, which is then applied in the testing stage to compute the likelihood of a new sequence being normal. A leave-one-out process is used to create subformations of the target observation sequence and the quality of the centre pixel is examined based on how similar the observation sequence without the centre pixel is relative to the mean of the subformations. This is described in more detail in subsection 3.2.

Let $I^t_{\mathbf{x}}$ represent the image intensity value at pixel location $\mathbf{x}$ at frame t. We extract intensity values at corresponding position $\mathbf{x}$ across frames temporally as a time series, i.e $\{I^t\}_{\mathbf{x}}$. We specify θ as an HMM containing Q states. The transition structure of a normal sample model is assumed to contain 5 stages. These correspond to states at a position $\mathbf{x}$: background, intermediate stage between background and foreground, foreground, intermediate stage between foreground and background, and background again (possibly different to that initially at $\mathbf{x}$). At each stage it is possible to jump by 0, 1, or 2 steps to the next state (see Figure 1). The state sequence goes from left to right and then iterates so that it is possible to model more complicated cases, such as multiple moving objects passing a pixel one after another.

For HMM θ, we define $\mathbf{O} = \{o_n, n = 1, \ldots, N\}$ as the set of observations where N is equal to the size of the discrete observation space. Observations o_n could be any kind of image features, such as intensity values, local variance and so on - in this work we use temporal absolute intensity differences for grayscale image sequences and temporal absolute Value differences in the HSV colour space for colour ones. Then, let $\{o(k)|o(k) \in \mathbf{O}, 1 \leq k \leq K\}^t_{\mathbf{x}}$ (abbreviated to $\{o(k)\}^t_{\mathbf{x}}$) be the sequence of observations centred at pixel $\mathbf{x}$ at time t for

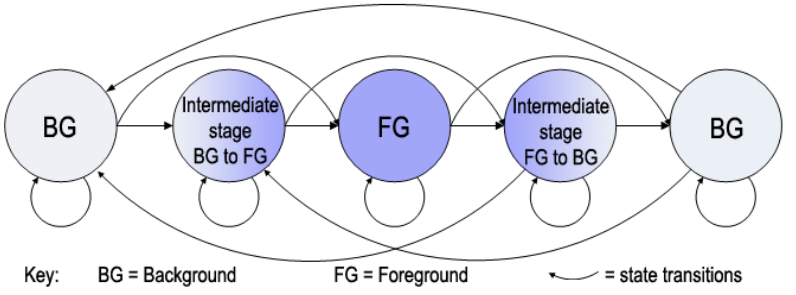

Figure 1: Graphical illustration of state transitions of a 5-state HMM in our application.

length K. The observation sequences are extracted from time series $\{I^t\}_{\mathbf{x}}$ within the range $[t-(\frac{K-1}{2}),t+(\frac{K-1}{2})]$. All observation sequences and state sequences share the same fixed length K at both training and detection stages. In a similar manner, let $\mathbf{S}=\{s_m,m=1,\ldots,Q\}$ be the set of states of pixels and $\{s(k)|s(k)\in\mathbf{S},1\leq k\leq K\}^t_{\mathbf{x}}$ (abbreviated to $\{s(k)\}^t_{\mathbf{x}}$) be the state sequence.

The parameters of our HMM model are $\lambda_\theta=(\pi,A,B)$: start probability $\pi=\{\pi(m),m=1,\ldots,Q\}$ which states the probability of $s(1)$ being s_m, transition probability matrix $A=\{a_{lm},l,m=1,\ldots,Q\}$ which states the probability of transition from current state s_l to next state s_m and emission probability $B=\{b_m(o_n),m=1,\ldots,Q,n=1,\ldots,N\}$ which states the probability of the observation o_n given the current state s_m. The initial estimation of these model parameters in our training stage is set using a random distribution.

3.1 Training stage

The training data consists of observation sequences computed from time series $\{I^t\}_{\mathbf{x}}$ with the same fixed length K. Different values of K for the optimal length of the observation sequences were examined and $K=13$ was found to give the most optimal results across our data set. A detailed comparison of different values of K is provided in section 5. Similarly for Q, different numbers of states and transitions ranging from 2 to 7 were experimented with and $Q=5$ provided the best overall detection result. The value $Q=5$ is logically more plausible given what it represents (as outlined above and in Figure 1). The training data was extracted at random positions from 10 different types of archive film (5 grayscale and 5 colour image sequences). In total, 207,561 observation sequences were used for training the HMM θ. The estimation of the parameters for our 5-state HMM was optimized by maximizing $P(\{o(k)\}^t_{\mathbf{x}}|\lambda_\theta)$ through an iterative procedure until convergence, using Baum-Welch's method [13].

3.2 Detection stage

The training stage results in an HMM which models the normality of pixel sequences. In the detection stage, we first apply this model to compute the likelihood of an observation sequence being normal, i.e. $P(\{o(k)\}^t_{\mathbf{x}}|\lambda_\theta)$. We then measure how the likelihood of this observation sequence (arising from normal data) varies if each single observation within it was missing, one at a time in a leave-one-out fashion. Thus, we will obtain a set of likelihoods

for each observation sequence. The pixel at the centre of the observation sequence can then be marked as a defect, if the likelihood of the observation sequence without the centre pixel is larger, by a certain degree, than the average of all leave-one-out likelihoods computed on the observation sequence. Formally, this is implemented as follows.

As in the training stage, we extract from the time series $\{I^t\}_{\mathbf{x}}$, a test observation sequence $\{o(k)\}^t_{\mathbf{x}}$ centred at candidate pixel $\mathbf{x}$ with observation $o(c)$ for each image pixel location. For every element in $\{o(k)\}^t_{\mathbf{x}}$, we define a new observation sequence indexed by h that does not include the element $o(k)$ itself, i.e. $\{o(h), h \neq k)\}^t_{\mathbf{x}}$. This will result in K observation sequences of length $K-1$. We can then obtain (for each of these K observation sequences) the likelihood of the observation sequence $\{o(h), h \neq k\}^t_{\mathbf{x}}$ arising from normal data,

$$V^t_{\mathbf{x}}(k) = P(\{o(h), h \neq k)\}^t_{\mathbf{x}} | \lambda_\theta) = \sum_m P(\{o(h), h \neq k\}^t_{\mathbf{x}}, s(k') = s_m | \lambda_\theta) = \sum_m \alpha_{k'}(m)\beta_{k'}(m) \tag{2}$$

where $k = 1, \ldots, K$, $k' = k-1$, and $\alpha_y(m), \beta_y(m), y \in \{k, k'\}$ are defined using the Forward-Backward procedure [15]:

$$\begin{aligned} \alpha_y(m) &= P(\{o(g), g = 1 \ldots y\}^t_{\mathbf{x}}, s(y) = s_m | \lambda_\theta) \\ \beta_y(m) &= P(\{o(g), g = y+1 \ldots K\}^t_{\mathbf{x}} | s(y) = s_m, \lambda_\theta) \end{aligned} \tag{3}$$

with $\alpha_0(m) = P(\{o(g), g = 2\}^t_{\mathbf{x}}, s(2) = s_m | \lambda_\theta)$, and $\beta_0(m) = P(\{o(g), g = 3 \ldots K\}^t_{\mathbf{x}} | s(2) = s_m, \lambda_\theta)$.

Complex situations like intensity level changes caused by motion can result in a high value of $V^t_{\mathbf{x}}(k)$. We compute the mean of all $V^t_{\mathbf{x}}(k)$ values to average out the effect of such situations.

$$u^t_{\mathbf{x}} = \frac{V^t_{\mathbf{x}}(c)}{\frac{1}{K}\sum_{k=1}^K V^t_{\mathbf{x}}(k)} \tag{4}$$

After computing $u^t_{\mathbf{x}}$ for every pixel $\mathbf{x}$ in frame t, we obtain the likelihood map $U^t = \{u^t_{\mathbf{x}}\}$ for all $\mathbf{x}$ in frame t. Finally, any pixel $\mathbf{x}$ is marked as a defect in a global frame binary defect map $D^t = \{d^t_{\mathbf{x}}, d^t_{\mathbf{x}} \in \{0,1\}\}$ if $u^t_{\mathbf{x}} > \tau_\theta$ where τ_θ is a threshold (see later for discussion of how this threshold is determined).

4 Elimination of false alarms

The HMM model performs extremely well in locating true defects, however it is rather sensitive to scene motion leading to false positives. As shown in (4), we compute the mean of all $V^t_{\mathbf{x}}(k)$ values (i.e. the likelihood of all observation sequences) to average out the effect of intensity level transitions caused by motion. However, if the length of such transitions compared to the entire state sequence is short, as true defects are, then false alarms arise in or around moving regions caused by object and/or ego motion. The middle column in Fig. 2 shows examples of applying the model with the resulting defect maps overlaid on the original frames (shown in the first column), with the true defects marked in green and the false alarms marked in red.

This over-detection followed by false positive elimination is preferred to under-detection and its consequences. In order to identify and remove the false alarms, we apply a two-stage process enforcing (a) spatial continuity and (b) temporal correlation constraints.

For those false alarms that locate around the edges, such as the red pixels around the TV presenter's head in the top row example, strong spatial correlation with their neighbors may

Figure 2: Example results: (left) original images (middle) HAFID results before false alarm elimination, and (right) after false alarm elimination.

be found. In such cases local smoothness can be exploited by modeling the defect map D^t and the likelihood map U^t with MRFs to encourage grouping defects into connected regions while removing false positives by propagating neighbouring non-degraded pixel locations (see subsection 4.1).

For those false alarms that make up an entire moving region, for example, the shadows in the curtain folds in the bottom row example in Fig. 2 which leave the scene as the camera pans and zooms in towards the girl, no relationship with other pixels may be found unless we trace forwards and backwards on the temporal axis. The pyramidal Lucas-Kanade feature tracker [2] is adopted here in order to impose temporal constraints (see subsection 4.2).

4.1 MRF modelling

In [12], Morris adopted an Ising model to represent the prior of what he referred to as his *detection frame* (effectively an initial defect map). Gibbs sampling with annealing was then applied to achieve the maximum a *posteriori* (MAP) configuration of the defect map given the image intensities from two adjacent motion compensated image frames. Positions in his final defect map were marked if discontinuities were shown on both adjacent frames. In this work, in contrast to Morris's initial zero-valued detection frame, D^t becomes our initial defect map, effectively providing advanced-stage prior information. False alarms are then eliminated iteratively by computing the MAP configuration of D^t given the likelihood map U^t. Thus, again unlike Morris [12], who investigated intensities at this point, we use the original likelihood map values in U^t to support the MAP estimation of D^t.

This process is implemented as follows. According to Bayes' theorem:

$$P(D^t|U^t) \propto P(U^t|D^t)P(D^t) \tag{5}$$

The joint probability distribution of U^t modelled with a MRF is equivalent to a Gibbs distribution. The function $\phi(\cdot) = (\cdot)^2$ is used to denote the potential for all possible connected

2-element cliques in an 8-connected neighbourhood. For each defect position in map D^t, we compute the probability of a pixel having value $u^t_{\mathbf{x}}$ as a function of all its spatial neighbourhood ($N^t_{\mathbf{x}}$) pixel likelihoods and (previous frame) temporal neighbour $u^{t-1}_{\mathbf{x}}$. So the joint probability distribution of U^t given D^t is:

$$P(U^t|D^t) = \frac{1}{Z_{U^t}} exp(-\sum_{\mathbf{x}}[\alpha' \sum_{\mathbf{x}' \in N^t_{\mathbf{x}}} \phi(u^t_{\mathbf{x}} - u^t_{\mathbf{x}'}) + \alpha(1-d^t_{\mathbf{x}})\phi(u^t_{\mathbf{x}} - u^{t-1}_{\mathbf{x}})]) \quad (6)$$

where Z_{U^t} is a normalizing constant and α', α are weights. The prior of defect map D^t is:

$$P(D^t) = \frac{1}{Z_{D^t}} exp(-\sum_{\mathbf{x}}[-\beta_1 \sum_{\mathbf{x}' \in N^t_{\mathbf{x}}} \delta(d^t_{\mathbf{x}} - d^t_{\mathbf{x}'}) + \beta_2 \delta(1-d^t_{\mathbf{x}})]) \quad (7)$$

where $\delta(\cdot)$ is the delta function, β_1, β_2 are weights and Z_{D^t} is also a normalizing constant. Finally, combining (6) and (7), the *a posteriori* likelihood function is:

$$P(D^t|U^t) \propto \frac{1}{Z^t} exp(-\sum_{\mathbf{x}}[\alpha(1-d^t_{\mathbf{x}})(u^t_{\mathbf{x}} - u^{t-1}_{\mathbf{x}})^2 - \beta_1 \sum_{\mathbf{x}' \in N^t_{\mathbf{x}}} \delta(d^t_{\mathbf{x}} - d^t_{\mathbf{x}'}) + \beta_2 \delta(1-d^t_{\mathbf{x}})]) \quad (8)$$

where $Z^t = Z_{U^t} Z_{D^t}$. Gibbs sampling with annealing [5] is applied to compute the MAP configuration for eliminating false alarms. We set $\beta_1 = 1$, as suggested in [19], and apply a similar parameter estimation procedure as [12] for (α, β_2). The rightmost, top row image of Fig. 2 shows the TV presenter scene after false alarm elimination using this approach.

4.2 Motion tracking

Some false alarms make up an entire (but small) moving region, and hence we look for temporal correlation constraints. We apply pyramidal Lucas-Kanade motion tracking [2] on pixels corresponding to map D^t positions across several frames before and after the current frame to determine the stability of the pixels being tracked. If the track fails, then the position in D^t is left unchanged, otherwise it is eliminated as a false positive. The rightmost image of the bottom row of Fig. 2 shows an example of a scene after false alarm elimination using this approach.

5 Experiments

The specificity and sensitivity of the proposed method HAFID-STC is measured with reference to handlabeled groundtruth produced from 30 film sequences totalling 580 frames (note this data set is entirely different from the training data). These include grayscale, colour, indoor, outdoor, slow and fast motions, and real scenes and cartoons.

The ROC graph in Figure 3 shows a comparison of HAFID-STC against those of four commonly used and/or state-of-the-art techniques: SDIp [10], Morris's MRF based defect detector [12] (referred to as Morris95), Ren and Vlachos's recent work [18] (referred to as RV07) and a Bayesian defect detection framework [8] (referred to as Kokaram04), all briefly described earlier. These methods were all tuned for optimal performance. The results from using only our HMM based detector HAFID (i.e. the results in D^t obtained from thresholding U^t after (4)) for different window sizes K are also shown. The correct detection ratio (sensitivity) is plotted against the false alarm ratio (1-specificity) computed from the

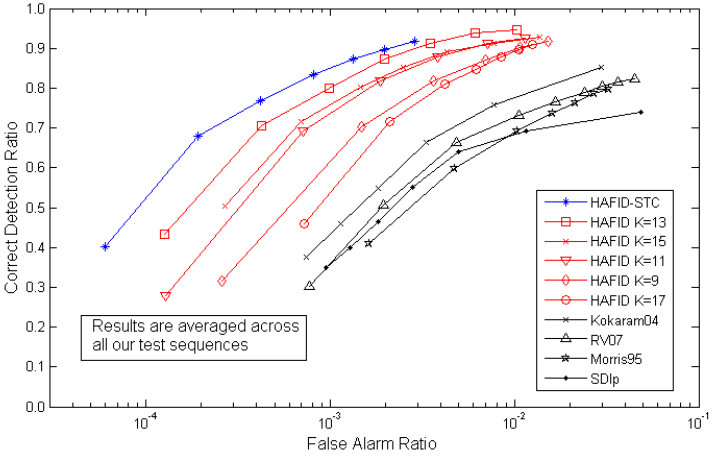

Figure 3: ROC graph shows a comparison of HAFID-STC against four well known or current state-of-the-art techniques [8, 10, 12, 18], averaged across our entire test data set.

average from the 30 test sequences. For each algorithm, its key parameters are varied to measure its performance for the ROC graph.

For HAFID the threshold τ_θ was varied while for HAFID-STC, i.e. the full proposed method, we find the optimum α and β_2 for each τ_θ which was varied in the same manner as for HAFID. As shown in Fig. 3, HAFID comfortably outperforms all previous methods while HAFID-STC achieves the best results overall.

Figure 4 shows a comparative visual example for a sample degraded frame. SDIp detected 92.1% of the defects but also produced 717 false alarm pixels (out of a total frame size of 136704 pixels). Morris95 and RV07 were able to achieve correct detection rates of 93.8% and 93.3% but still resulted in 674 and 725 false detections respectively. Kokaram04 produced far fewer false alarms (253) but only detected 86.7% of the true defects. The HAFID method was better at both detecting more true positives, i.e. 94.6%, and fewer false alarm pixels at 97 only, while the full proposed method HAFID-STC improved the result further by reducing the false alarms down to 50 pixels.

Table 1 shows a comparison of the computational speed of all the methods in terms of average time per frame[2] in seconds. All implementations were coded and computed in MATLAB on a laptop with Intel Centrino 1.6 GHz and 1GB RAM. The proposed algorithm is somewhat slower than SDIp, considering a longer temporal range is investigated to help determine defects, but it is a lot more accurate and also outperforms all the other methods.

Table 1: Averaged computational speed for all methods

Method	SDIp	Morris95	RV07	Kokaram04	HAFID K=13	HAFID-STC
seconds	4	443	93	80	19	26

[2]The average frame size in our data is 480×356 pixels

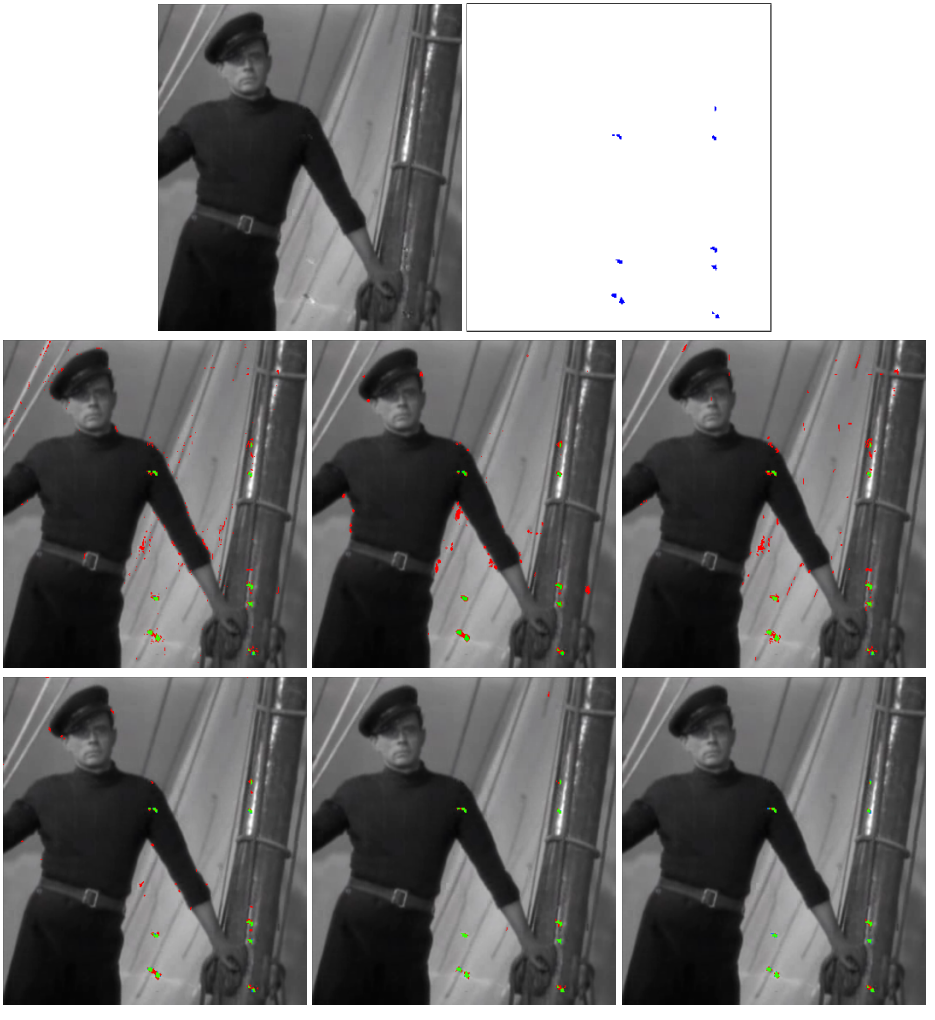

Figure 4: (top) Degraded frame and its groundtruth mask, (middle) detection results from SDIp, Morris95, RV07, and (bottom) results from Kokaram04, HAFID and HAFID-STC. Green: correctly detected defect; Red: false alarms; Blue: defects not detected.

6 Conclusion

We have presented an archive film defect detection scheme involving HMM modelling of temporal pixel sequences to obtain an initial defect map and then, using this map as a prior in an MRF scheme, to iteratively remove false positive defect candidates by examining spatial constraints followed by a motion tracking stage to remove more false positives based on temporal constraints.

In this work we have found that it is better to have an overzealous defect detector and then remove false positives, rather than apply a conservative method where not all true defects are found and extra steps would have to be implemented till a reasonable target is met.

The proposed method would fail to respond to a defective pixel if all pixels across a single observation sequence were defective pixels, although this rarely happens except for a continuous vertical line scratch. However, overall, the proposed approach performs much more accurately than the current state-of-the-art and is considerably faster too (except for SDIp which is not so accurate).

Acknowledgements
We thank Great Western Research, ITV and Bristol University for funding this project. We particularly thank Brian Hann from ITV for the supply of data and invaluable advice.

References

[1] J. Besag. On the statistical analysis of dirty pictures. *Journal of the Royal Statistical Society Series B*, 48:259–302, 1986.

[2] J. Y. Bouguet. Pyramidal implementation of the lucas kanade feature tracker. Technical report, OpenCV Documentation, Intel Corporation, Miroprocessor Research Labs, 2000.

[3] BRAVA. http://brava.ina.fr.

[4] M. Chong and D. Krishnan. An edge-preserving MRF model for the detection of missing data in image sequences. *IEEE transactions on Signal Processing Letters*, 5(4): 81–83, 1998.

[5] S. Geman and D. Geman. Stochastic relaxation, gibbs distributions, and the bayesian restoration of images. *IEEE Transactions on Pattern Analysis and Machine Intelligence*, 6:721–741, 1984.

[6] M.S. Hamid and S. Marshall. Fpga realisation of the genetic algorithm for the design of grey-scale soft morphological filters. In *Proceedings of International Conference on Visual Information Engineering*, pages 141–144, 2003.

[7] K. Hough and S. Marshall. Soft morphological filters applied to the removal of noise from cctv footage. In *Proceedings of IEE International Symposium on Imaging for Crime Detection and Prevention*, pages 61–66, 2005.

[8] A. Kokaram. On missing data treatment for degraded video and film archives: a survey and a new bayesian approach. *IEEE Transactions on Image Processing*, 13(3):397–415, 2004.

[9] A. Kokaram and S. Godsill. MCMC for joint noise reduction and missing data treatment in degraded video. *IEEE Transactions on Signal Processing*, 50(2):189–205, 2002.

[10] A. Kokaram and P. Rayner. System for the removal of impulsive noise in image sequences. *Journal of Visual Communication and Image Representation*, 1818(1):322–331, 1992.

[11] A. Kokaram, R. Morris, W. Fitzgerald, and P. Rayner. Detection of missing data in image sequences. *IEEE Transactions on Image Processing*, 4(11):1496–1508, 1995.

[12] R. Morris. *Image Sequence Restoration using Gibbs Distributions*. PhD thesis, Cambridge University, 1995.

[13] M. Nadenau and S. Mitra. Blotch and scratch detection in image sequences based on rank ordered differences. In *Proceedings of International Workshop on Time-Varying Image Processing and Moving Object Recognition*, pages 1–7, 1997.

[14] PrestoSpace. http://prestospace.org.

[15] L. Rabiner. A tutorial on hidden markov models and selected applications in speech recognition. *IEEE Proceedings*, 77(2):257–286, 1989.

[16] P. Read and M. Meyer. *Restoration of Motion Picture Film*. Butterworth Heinemann, 2000.

[17] J. Ren and T. Vlachos. Segmentation-assisted dirt detection for the restoration of archived films. In *Proceedings of British Machine Vision Conference*, volume I, pages 359–368, 2005.

[18] J. Ren and T. Vlachos. Efficient detection of temporally impulsive dirt impairments in archived films. *IEEE Transactions on Signal Processing*, 87(3):541–551, 2007.

[19] B. D. Ripley. *Statistical inference for spatial processes*. Cambridge University Press, 1988.

[20] P. Van Roosmalen. *Restoration of Archived Film and Video*. PhD thesis, Delft University, 1999.

[21] R. Storey. Electronic detection and concealment of film dirt. *Journal of Society of Motion Picture and Television Engineers*, pages 642–647, 1985.